Challenge Journal of Structural Mechanics

Research Article

Predicting shear strength in reinforced concrete deep beams through finite element modeling of diverse concrete materials

Erkan Polat [a,*], Gökhan Karaman [a]

[a] *Department of Civil Engineering, Munzur University, 62000 Tunceli, Türkiye*

ABSTRACT

This study investigates the prediction of the strength of reinforced concrete deep beams, critical components in urban infrastructure, by evaluating their load-carrying capacities through finite element modeling and nonlinear inelastic analyses using LS-DYNA software. Four widely used concrete material models were examined: Mat084/085, Mat159, Mat072R3, and Mat016. Analyses were conducted on two single-span and four double-span beams with varying reinforcement configurations and an aspect ratio of 1.0, based on well-documented experimental setups. Comparative analyses of force-displacement behavior and stress distributions revealed significant differences in shear strength predictions across the models, with Mat159 providing the most accurate results. These findings establish a reliable and cost-effective approach for predicting the capacities of deep beams, reducing reliance on extensive experimental testing. The study contributes valuable insights for improving strength predictions in critical infrastructure applications such as bridges and foundations.

ARTICLE INFO

Article history:
Received – October 12, 2024
Revision requested – November 19, 2024
Revision received – December 5, 2024
Accepted – December 16, 2024

Keywords:
Deep beams
Shear strength
Finite element modeling
LS-DYNA
Concrete material models

Citation: Polat E, Karaman G (2025). Predicting shear strength in reinforced concrete deep beams through finite element modeling of diverse concrete materials. *Challenge Journal of Structural Mechanics*, 11(1), 24–41.

1. Introduction

In an era of rapidly urbanizing cities, resilient structural elements like deep beams play an essential role in safeguarding critical infrastructure. Deep beams, with their unique load transfer mechanisms predominantly via shear, are vital components in the construction of resilient foundations, bridges, and high-rise buildings. Their ability to withstand significant stresses and distribute loads efficiently makes them indispensable in designing infrastructure capable of withstanding urban challenges, including seismic events, extreme weather, and increasing building loads driven by urban densification. Understanding the behavior and capacity of deep beams under various stress conditions is crucial to improving their design for urban resilience.

Deep beam design and analysis can be complex due to non-linear stress distributions and the potential for large shear forces, requiring specialized approaches like the strut-and-tie method for accurate assessment. Guidelines for various models and theories (e.g., truss model approaches, compression field theories, strut-and-tie models, etc.) for designing reinforced concrete deep beams to resist shear forces are included in ACI 318-19 (2019) and ASCE-ACI Committee 445 on Shear and Torsion (1998).

According to ACI 318-19 (2019), deep beams are defined as elements loaded on one face and supported on the opposite face, where compression and similar compressive elements may develop between loads and supports. Deep beams must be designed considering the nonlinear distribution of longitudinal strain over the

* *Corresponding author*. Tel.: +90-428-213-1794 ; E-mail address: erkanpolat@munzur.edu.tr (E. Polat)
ISSN: 2149-8024 / DOI: https://doi.org/10.20528/cjsmec.2025.01.003

depth of the beam. The net span-to-depth ratio ($2a/h$) of deep beams should not exceed 4, or in the case of a concentrated load, the ratio of the load's distance from the support (a) to the depth (h) should be less than or equal to 2. For the shear reinforcement, A_v should be greater than or equal to, $0.0025b_w s$ (where b_w represents the web width of the beam, and s denotes the spacing of the distributed transverse reinforcement). For the longitudinal reinforcement, A_{vh} should be greater than or equal to $0.0025b_w s_2$ (where s_2 is the spacing of the distributed longitudinal reinforcement). According to the CSA A23.3 (2004), beams with a net span-to-depth ratio of less than 2 are defined as deep beams. Deep beams are designed considering nonlinear stress distributions, lateral torsional buckling, and increasing stresses at the nodes of reinforcements. The use of the Strut-and-Tie Model (STM) method is indicated as necessary for the design of deep beams.

In the literature, there are many analytical and numerical studies aimed at predicting the load-carrying capacities of deep beams. Due to the discontinuity in the stress distribution in deep beams, complex finite element methods (FEM) are often used for modeling and analyzing their behavior. LS-DYNA is one of the most frequently used programs for analysis in civil and structural engineering applications. It has proven to be an essential tool for structural analysis, particularly in predicting dynamic responses and failure mechanisms in complex structures (Markovich et al. 2011; Imani et al. 2015; Jiang and Zhao 2015; Youssf et al. 2015; Polat and Bruneau 2017, 2018; Grassl et al. 2018; Polat 2020a, 2020b, 2022a, 2022b; Polat et al. 2021; Zhao et al. 2021; Polat and Polat 2024; Tang et al. 2024). The program library contains many concrete materials, which can be used with complex parameter inputs, but are generally utilized by users through the default parameter generation option. In this study, the predictability of the capacities of experimentally tested deep beams using the default concrete parameter creation option in concrete materials, often preferred in structural engineering applications, is investigated using the LS-DYNA program.

In this numerical study, four different concrete material models in LS-DYNA – Mat084/085 (Winfrith), Mat159 (CSCM), Mat072R3 (KCC), and Mat016 (Pseudo-TENSOR) – are utilized to analyze the load-carrying capacities of reference deep beams. The study aims to identify the most accurate model for predicting these capacities, analyze stress formations and distributions within the concrete, and assess axial force demands in beam reinforcements for each material model. By doing so, the research seeks to establish a reliable method for estimating the capacity of deep beams, which are typically costly to test experimentally, while enabling the exploration of various beam parameters, such as aspect ratios and reinforcement configurations, without requiring extensive experimental studies.

The reference models are based on the experimentally tested deep beams documented by Rogowsky et al. (1986), where their behavior was thoroughly analyzed. The significance of Rogowsky et al.'s work is well-established and validated by its inclusion in the Commentary R9.9.1.1 of ACI 318-19 (2019) which highlights this study, along with others (Marti 1985; Schlaich et al. 1987), as foundational for understanding deep beam behavior. The continued relevance of this work underscores its impact on contemporary engineering practices, particularly in the design and evaluation of deep beams and their load-carrying capacities.

Additionally, the study contributes novelty by comparatively evaluating these concrete material models to determine the most effective approach for finite element simulations of deep beams. This focus addresses a significant gap in the literature and provides insights into model performance, enhancing reliability in predictions for critical infrastructure applications. By bridging experimental results with advanced numerical modeling, this research offers a practical, cost-effective solution for designing and analyzing deep beams in structural engineering.

Moreover, the study provides a novel contribution by comparatively evaluating these concrete material models to determine the most effective approach for finite element simulations of deep beams. This research highlights the application of four widely used concrete material models in LS-DYNA, a powerful tool for advanced numerical simulations. By focusing on the comparative performance of these models in predicting the behavior of deep beams, the study offers an understanding of their suitability for finite element analysis of similar engineering structures. While prior studies have explored deep beam behavior experimentally, limited work has systematically evaluated these specific material models in the context of deep beam shear strength predictions. This research, therefore, offers practical insights into the use of advanced material models and simulation tools for structural analysis, establishing a reliable and cost-effective approach for analyzing deep beams in critical infrastructure applications.

2. Literature Review

The literature includes a wide range of experimental, analytical, and numerical studies that have employed various methods to predict the strength of deep beams. These diverse approaches are designed to enhance the accuracy and reliability of predictions related to the performance and safety of deep beams in construction and engineering. In this section, key research studies are summarized to highlight the advancements in this field.

Rogowsky et al. (1986) conducted experimental analysis of the shear behavior of reinforced concrete deep beams. The study examined 24 beams, including 7 simply supported and 17 two-span continuous deep beams, with different shear span-to-depth ratios and web reinforcement patterns. The experiments observed a range of behaviors from brittle to ductile, depending on the presence and amount of vertical web reinforcement. The results indicated that horizontal web reinforcement had no significant impact on capacity. The ACI Building Code's predictions for continuous deep beams and those with horizontal shear reinforcement were found to overestimate strength. This study is crucial for understanding the impact of reinforcement patterns on the strength

and behavior of deep beams. Arabzadeh (2020) studied on the impact of different boundary conditions on the behavior of RC deep beams. The study used experimental and theoretical analysis of 43 deep beams with various reinforcement arrangements and boundary conditions. The study concluded that boundary conditions significantly affect ultimate loads, failure modes, and deflections. The study also proposed a method for analyzing deep beams, which shows good agreement with experimental data. Collins et al. (2008) examined the research on shear behavior in beams tested in the past and assessed 1849 tests and evaluated the safety of shear provisions in North America. It was argued that current ACI shear provisions may be unconservative for members with larger effective depths or higher stresses in longitudinal reinforcement. Chen et al. (2019) presented a comprehensive study on the shear strength of reinforced concrete deep beams. The research focused on both simple and continuous deep beams, analyzing their structural behavior, particularly in terms of shear strength. The study employed a combination of experimental observations, nonlinear finite element analyses, and a review of existing test databases. Chen et al. (2020) presented a comprehensive study on shear-transfer mechanisms and strength modeling of reinforced concrete (RC) continuous deep beams. The study involves detailed experimental observations, numerical analysis using finite element methods, and theoretical considerations of various shear-transfer mechanisms. Zargarian and Rahai (2022) conducted a study on continuous RC deep beams strengthened with carbon fiber reinforced polymer (CFRP) strips. The study included experimental and numerical analyses, focusing on the effect of different shear span-to-overall depth ratios and CFRP strip arrangements. Finite element analyses of the tested specimens were developed to simulate experimental specimen behavior. Gedik et al. (2012) investigated the impact of stirrups on deep beam shear failure mechanisms using an analytical tool 3-D Rigid-Body-Spring Model (RBSM). The study examined stress distribution, deformations, crack patterns, and stirrup strain, providing insights into deep beam shear failure mechanisms influenced by stirrups. Ma et al. (2023) explored a data-driven model to predict the shear strength of reinforced concrete (RC) deep beams. They utilized machine learning (ML) algorithms and interpretable models, to compare the performance of different ML models in predicting shear strength. Li et al. (2023) introduced a new shear strength determination method for reinforced concrete (RC) deep beams using a statistical approach. The study employed the Bayesian-Markov Chain Monte Carlo (MCMC) method to establish a new shear prediction model and improve existing deterministic models.

3. Description of the Reference Deep Beam Models

Within the scope of this study, experimental study of Rogowsky et al. (1986) carried on two single-span and four double-span reinforced concrete deep beams with an aspect ratio of 1.0 were considered. In the experimental study, various combinations of vertical and horizontal reinforcement on the behavior of these beams were examined, failure modes and the influence of different reinforcement configurations and quantities on the structural performance of the beams were investigated.

Fig. 1(a-f) shows the reinforcement layout in the reference beams considered in this study. As reported by Rogowsky et al. (1986) the reinforcements were designed in accordance with the ACI Code Sections 11.8.8 and 11.8.9 (ACI 318-83 1983), adhering to both the minimal and maximal vertical and horizontal reinforcement limits: the quantity of shear reinforcement varied from the minimum requirement of 0.0015, as specified by the code, to a value four times greater than this minimum, and the primary flexural reinforcements were carefully chosen to ensure that shear was the predominant mode of failure.

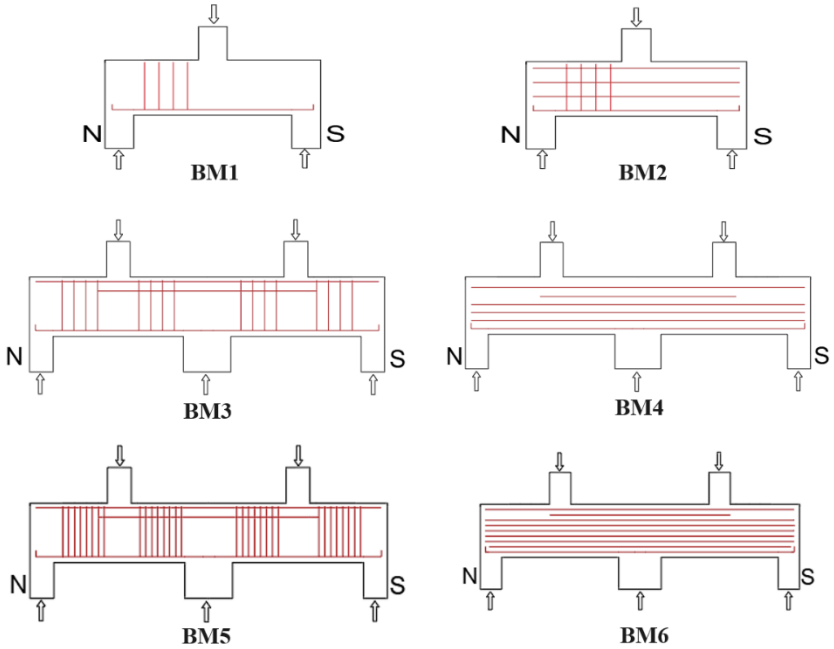

Fig. 1. Reinforcement layout of the reference beams: (a) BM1; (b) BM2; (c) BM3; (d) BM4; (e) BM5; (f) BM6.

The original nomenclature for the beams is maintained in the study. In Fig. 1 'N' and 'S' represent the north and south sides of the beams. As shown in the figure BM1 has stirrups only on the left shear span and no stirrups on the right; BM2 has horizontal body reinforcement at both spans and shear reinforcement only at the left span; BM3 is a continuous beam and has shear reinforcement at all the four span; BM4 is a continuous beam with body reinforcement passing through all spans but does not have shear reinforcement; BM5 is a continuous beam and has heavy shear reinforcement across the four shear spans; BM6 is a continuous beam with a high amount of body reinforcement, but it does not have shear reinforcement.

Table 1 details the properties of concrete and reinforcement used in the test beams. The reinforcement included two types: stirrups with a diameter of 6 mm, and 20M (19.5 mm diameter) bars for the bottom reinforcements. The properties of the reinforcement are given in Table 2. The beams had concrete strengths between 26.1 and 36.9 MPa. The maximum aggregate size used was 10 mm. Fig. 2 presents the typical dimensions of the tested deep beams, both single-span and double-span. The dimensions specified are A = 750 mm, B = 300 mm, C = 450 mm, and D = 1000 mm.

Table 1. Concrete and reinforcement properties of the tested beams (Rogowsky et al. 1986).

Beam models	f_c' MPa	Top reinforcement			Bottom reinforcement			Web reinforcement	
		Number-diameter	$A_s f_y$ (kN)	d (mm)	Number-diameter	$A_s f_y$ (kN)	d (mm)	Number of stirrups	Number of horizontal bars
1	26.1	-	-	-	6-20M	114	950	4	-
2	26.8	2-6 mm	16.2	980	6-20M	114	950	4	4
3	28.9	4-20M	114	950	3-20M	114	975	4	-
4	28.5	4-20M	114	950	3-20M	114	975	-	4
5	36.9	4-20M	121	950	3-20M	121	975	16	-
6	35.8	4-20M	121	950	3-20M	121	975	-	12

Table 2. Properties of steel reinforcement used in tested beams (Rogowsky et al. 1986).

Bar diamater (mm)	$A_s f_y$ (kN)	Yield strain	A_s (mm²)	E (MPa)	f_y (MPa)
20	114	0.00185	302	205400	377-380
6	16.2	0.00210	37.8	273000	428-573

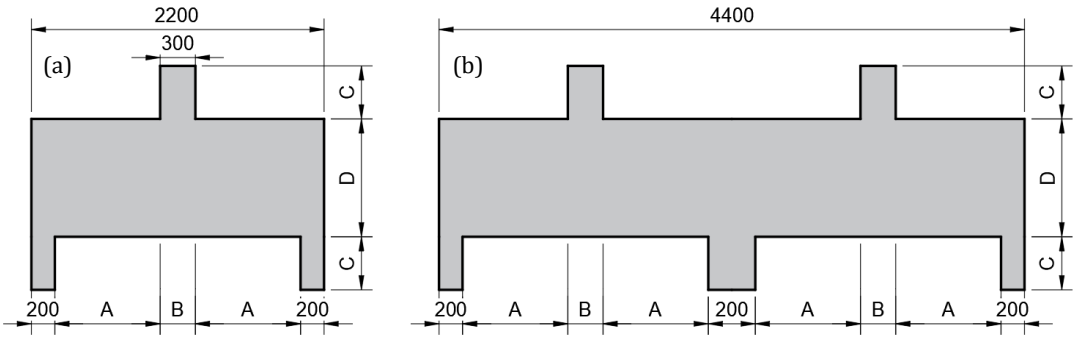

Fig. 2. Typical dimensions of the reference beams: (a) Single-span; and, (b) Double-span.

4. Summary of Experimental Observations

The study of beams BM1 to BM6 showed different failure patterns. BM1 had significant early cracks and a brittle failure due to strong concrete struts. BM2 failed from concrete crushing at strut ends, with early strut formation. BM3, moderately ductile, failed due to concrete strut failure, with major cracks appearing under significant load. BM4 exhibited clear strut formations and failed due to crushing at the strut's top. BM5 had major cracks and less pronounced struts, failing in shear compression at the strut's upper end. BM6, similar in cracking, also failed due to shear compression at the struts' upper ends, with some handling damage noted.

Experimental observations (Rogowsky et al. 1986) identified two main behavior patterns in deep beams. Beams without or with minimal web transverse reinforcement (stirrups) exhibited tied-arch action at failure, independent of the amount of horizontal body reinforcement. These beams, structured with minimal reinforcements, typically failed in a brittle manner following a tied-arch pattern. Conversely, beams with substantial amounts of transverse reinforcement demonstrated more ductile behaviors. This distinction highlights the significant impact of reinforcement type and amount on the failure characteristics of deep beams.

Although designing beams without stirrups is not permissible in practical applications, the referenced experi-

mental study, which forms the basis of this research, aimed to investigate the influence of reinforcement on beam behavior and strength rather than develop design strategies. Shear reinforcement was intentionally removed or omitted on one side of the beams to isolate and examine its impact on shear strength and structural behavior. Similarly, this study focuses on replicating those experimentally tested configurations using finite element models to validate the numerical approach against established experimental results and ensure its reliability in simulating such scenarios.

5. Description of Finite Element Modeling

5.1. Element and material models

In the modeling of the reference deep beams, LS-DYNA was used. In the modeling, the concrete part of the beam was represented by "Solid 1," an eight-node constant-stress solid element (standard solid element model in the software). The beam's transverse and longitudinal reinforcements, which in reality undergo deformations due to axial load, shear force, and bending moments, were modeled using two-node beam elements, known as "Beam 1." (default beam element model in the program).

In the modeling, the concrete elements (solid nodes) and reinforcement elements (beam nodes) were meshed similarly and coupled directly. This approach assumes a perfect bond between concrete and reinforcement, with no slip occurring at the interface. Such an assumption simplifies the modeling process and is a commonly used methodology for representing rebar in concrete structures in numerical simulations.

Additionally, there are constraint-based contact models available in LS-DYNA, such as the CONSTRAINED_LAGRANGE_IN_SOLID (CLIS) keyword, which can achieve similar coupling between concrete and rebar without requiring identical meshing. This method ties the displacement of reinforcement nodes to surrounding concrete nodes, effectively simulating perfect bond behavior. According to Tay et al. (2016), this approach is widely employed in reinforced concrete modeling and has been validated for both static and dynamic applications.

In this study, while a direct mesh coupling was used, CLIS could also have been an effective alternative. Both methods inherently rely on the assumption of perfect bond behavior, which aligns with the configurations and objectives of our research

In the numerical study, a single steel material model was employed for the reinforcements, and four distinct concrete models were utilized. These models include: Mat084/085 (Winfrith), Mat159 (CSCM), Mat072R3 (KCC), and Mat016 (Pseudo-TENSOR). Wu et al. (2012) examined these models' performance in capturing key concrete behaviors through single-element simulations and structural analyses under various load conditions and compared numerical responses with test data to assess each model's effectiveness in predicting actual structural responses. These materials were also used and compared in the analysis of composite plate shear walls (Polat and Bruneau 2018; Polat 2022a).

Mat003 plastic kinematic material model was used for the material modeling of the beam reinforcements. This model demonstrates a bilinear behavior, characterized by a unit strain-stress curve as illustrated in Fig. 3. The required parameters are the yield strength, the elastic modulus (E), the tangent modulus (E_t), and the hardening parameter (β).

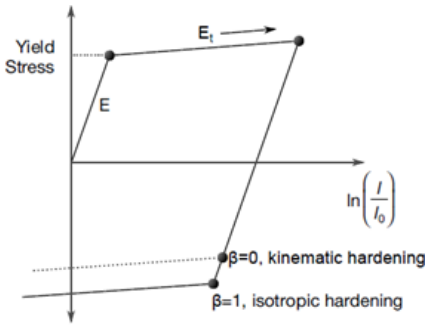

Fig. 3. Illustration of typical stress-strain curve of plastic kinematic material model.

The Mat003 plastic kinematic material model was chosen due to its simplicity and efficiency. This model requires minimal input parameters and is computationally efficient, reducing convergence issues. Given the lack of detailed steel component test history in the reference study and the focus of this research on predicting ultimate strength rather than the complete load-deformation behavior, Mat003 was deemed appropriate for the numerical modeling of beam reinforcements.

The Winfrith Concrete material in the software program is represented by two separate material models, Mat084 and Mat084/085. The Mat084 model includes a specific formulation designed for structural reinforcement. In contrast, the Mat084/085 lacks a formulation tailored for structural reinforcement (LSTC 2017). For Mat084/085 the amount of reinforcement must be specified in the analysis model using different elements through direct, one-to-one modeling. This approach allows for a more detailed and accurate representation of the reinforcement within the structural analysis. The formulation of this material is based on the research of Broadhouse and Neilson (1987) and Broadhouse (1995). This model is commonly employed in the structural modeling of concrete under diverse loading conditions. Its popularity stems from the minimal input requirements, which align closely with the properties of concrete typically used in engineering applications. A notable feature of this material model is its capability to accommodate crack planes in three directions per element (Wittmann et al. 1988). This feature enables the visual simulation of crack formation in analysis results. The essential material parameters required for this model are tangent modulus, poisson's ratio, uniaxial compressive strength, uniaxial tensile strength, crack width, aggregate size.

The Mat159 model, also known as Continuous Surface Cap Model (CSCM), is one of the most commonly used concrete models in LS-DYNA. Users have the option to input their own material properties for normal strength

concrete or request default material properties (LSTC 2017). This model is noted for its efficiency in simulating key concrete properties with minimal user input. The parameters required for the default material properties are uniaxial compressive strength, and aggregate size. Evaluation of this material model has been studied by many researchers (Murray et al. 2007; Winkelbauer 2015; Novozhilov et al. 2022)

Mat072R3 material model is also known as the Karagozian & Case Concrete (KCC) Model and utilizes three shear failure surfaces (LSTC 2017). The foundations of this concrete material model are based on the Pseudo-TENSOR Model (Material Type 16). The latest version, referred to as Rel3 or Version III, generates the required concrete material parameters used in this study based on simple concrete properties. The model is based on partially associative plasticity theory and has the ability to replicate a wide range of concrete behaviors, including hardening, softening, rate effects, confinement, shear dilatancy, and fracture. The model's effectiveness under various loading conditions has been demonstrated by researchers (Wu and Crawford 2015).

The Mat16 model, being a pseudo-tensor model, is particularly suited for materials that exhibit complex mechanical responses, including non-linear behavior, anisotropy, and rate dependency. The material has been used to analyze embedded steel-reinforced concrete structures subjected to impulsive loads. This model is highly suitable for the application of standard geological models such as the Mohr-Coulomb yield surface with the Tresca limit (LSTC 2017).

5.2. Definition of finite element analysis

Fig. 4 shows the finite element models developed for the BM1 and BM3 beams, illustrating the concrete and reinforcement components separately. The analyses were conducted using displacement-controlled loading. Fig. 5 presents the displacement curve established for the analysis, where the horizontal axis (abscissa) represents time, and the vertical axis (ordinate) indicates displacement in millimeters. A displacement of 10 mm is characterized as a linear increment over a 1-second time interval. In the numerical model, this displacement was uniformly applied to the top surface nodes of the column at the mid-span of the beam. Nonlinear analysis was executed using the implicit solution algorithm in the software. In this solution approach, the predefined displacement curve is applied in loading steps (*dt*) of 0.001 seconds.

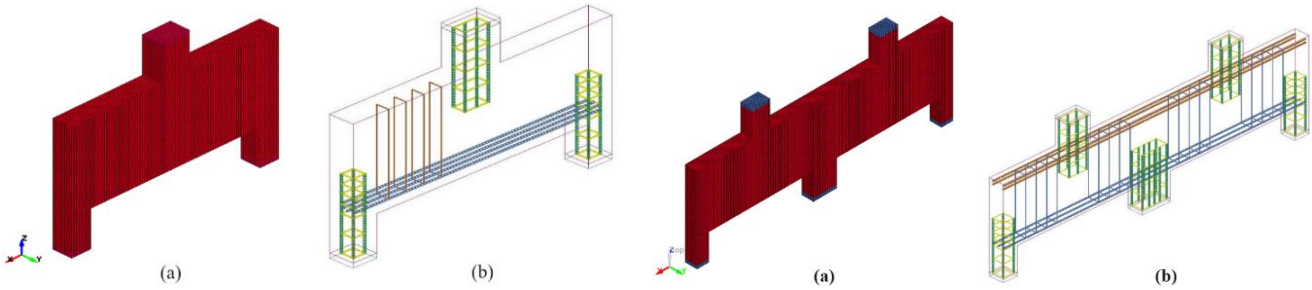

Fig. 4. Finite element models for BM1 and BM3: (a) Concrete part; (b) Reinforcement layout.

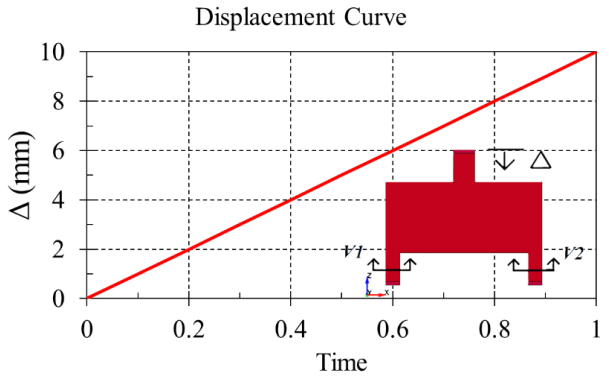

Fig. 5. Time-displacement curve used in analyses.

The tolerances used in the nonlinear analyses were set to the default values provided by LS-DYNA for implicit simulations to ensure consistent and reliable convergence. Specifically, the convergence tolerance for residual forces (TOL) was set to 1.0×10^{-9}. The minimum allowable time step size (Δt_{min}) was 1.0×10^{-8}, while the maximum allowable step size increment (Δt_{max}) was 0.004.

The shear strengths of the analysis models were obtained by adding up the shear forces generated in each span (left and right) of the beam. For instance, in the numerical model, the shear force demand for the left span of the beam model was determined by measuring the axial force demand (in the *z* direction) at a cross-section located at the beam's left support. Likewise, the shear force demand for the right span was ascertained by measuring the axial force demand at a cross-section at the right support. The overall shear carrying capacity of the numerical model was calculated as the sum of these two support reactions (i.e., V1 + V2).

It should be noted that a convergence study was conducted to establish the appropriate element sizes for the numerical beam model. Considering the distribution of transverse and longitudinal reinforcements and their spacings within the concrete of the beam, two element sizes were evaluated: 50 mm and 25 mm. These sizes were selected to enable as accurate as possible modeling of the reinforcements, resembling the actual tested specimen. The nodes of the beam elements used for reinforcements were aligned with the nodes of the solid elements, allowing the reinforcement to be coupled in dis-

placements with the concrete. This was achieved by merging the mutual nodes, ensuring that the reinforcement elements and the concrete elements moved in a dependent manner. To facilitate this integration, the dimensions of the reinforcement beam elements were made identical to those of the solid elements, that is, 50 mm or 25 mm in length.

Note that the element sizes used in this study (50 mm and 25 mm) were chosen considering the geometrical dimensions of the beam, the layout of the main and shear reinforcement, and the spacing between the rebars. Using finer meshes would result in excessively short beam elements for the reinforcement, given the 20mm diameter of the rebar. This could introduce numerical inaccuracies and undesired effects in the modeling of reinforcement behavior. Additionally, finer mesh resolutions would significantly increase computational cost. While intermediate sizes between 50mm and 25mm could improve robustness, the current configurations were deemed sufficient for accurately predicting ultimate strength within the scope of this study.

The model was set up as a simply supported beam with fixed boundary conditions at one end and roller support at the other, restricting vertical and transverse displacements while allowing longitudinal translation. Prescribed displacements were applied at the load application points. For the mesh sizes used, the total number of degrees of freedom (DOF) was approximately 78,000 for the 50mm mesh and 264,000 for the 25mm mesh. The beam reinforcements were modeled using beam elements coupled to the concrete solid elements through a constraint-based coupling method to simulate a perfect bond. The concrete was represented with the Mat084 material model, and the reinforcement with the Mat003 plastic kinematic material model. Hourglass control was applied to maintain numerical stability.

Fig. 6 displays the shear force-deflection curves derived from the nonlinear inelastic analysis results of the numerical beam models with two distinct mesh sizes. Additionally, the figure includes the experimentally determined maximum shear force capacity of the reference beam for comparison purposes. The findings from these outcomes reveal that the analysis result obtained with the model featuring a 50mm mesh size exhibited a strength that surpasses the actual beam strength upon comparison. Conversely, the analysis results from the model with a 25 mm mesh size exhibited a strength lower than the former and its results closely aligned with the actual beam's maximum shear strength.

It should be noted that the observed jumps in Fig. 6 are a result of the behavior of the numerical model during the nonlinear analysis, particularly in relation to the concrete material model (Mat084) used in the convergence study. The Mat084 concrete model has the ability to simulate concrete cracking, which results in the formation of sudden shear cracks in the beam. This leads to abrupt changes in the structural response, causing the sudden drops in the observed beam strength displayed in Fig. 6.

However, it is important to note that the finite element (FE) simulation used in this study does not explicitly model concrete failure or element erosion. As a result, the model does not capture the softening behavior of the concrete or the subsequent beam failure after reaching the maximum strength. This limitation contributes to the sharp transitions observed in the load-deflection curves.

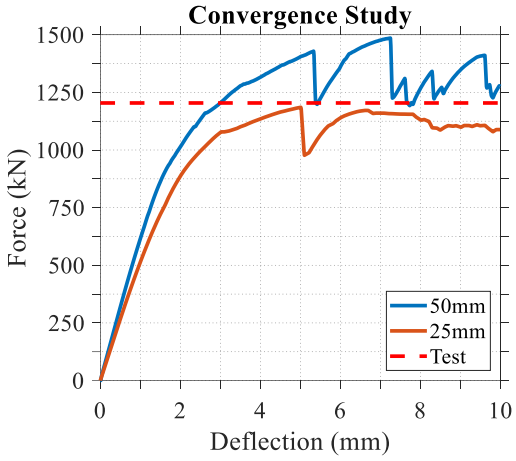

Fig. 6. Comparison of the numerical model results for the convergence study.

6. Finite Element Analysis Results

In this section, comparisons are made of the global load-displacement curves of beams subjected to nonlinear inelastic analyzes using different concrete materials, taking into account the experimentally measured beam strengths. Additionally, the axial force demands on the reinforcements for each model are examined. This approach allows for a comprehensive assessment of how different concrete materials affect the overall structural response of the beams, as well as the specific demands placed on the reinforcements under different material models.

It should be noted that comparing the overall beam behavior, such as force-displacement analysis, requires explicit modeling of not only the specimen but also the test setup itself. This is because the stiffness of the tested specimen can be influenced by various factors, such as deformation in the loading equipment, stiffeners, or slippage at the beam supports. Properly replicating these conditions in the FE model is a demanding task and requires careful calibration, including considerations such as friction between components, the modulus of elasticity of the concrete, and other parameters. Due to these complexities, no attempt was made to calibrate the stiffness of the numerical models or to replicate the entire nonlinear behavior of the specimens. Instead, the focus of the study was on predicting the ultimate strength of the beams, which is independent of these factors. The decision to prioritize ultimate strength stems from its inherent stability against variations in external testing conditions, ensuring a more robust comparison of material models.

The analysis results indicate that the beams exhibit a truss-like behavior within the concrete, characterized by the formation of diagonal compression struts. Fig. 7 presents the minimum principal stress contours for BM1 across the different concrete material models. These

contours highlight the development of diagonal compression struts, which are crucial for understanding the distribution of internal stress and overall structural performance of the beams. The stress contours for the Mat084 and Mat159 models are significantly more pronounced than those for the Mat072R3 and Mat016 models, reflecting the varying responses of the beams under the specified deflection. This distinction in stress contour prominence corresponds to the differing strengths retained by the beams under load. Specifically, the beams analyzed with the Mat084 and Mat159 models maintain a greater degree of strength, while those analyzed with Mat072R3 and Mat016 exhibit moderate to significant strength losses, respectively. In the case of the Mat072R3 model, there is a notable localized loss of minimum principal stress, which is attributed to the significant yielding of the shear reinforcements at the given deflection. This yielding alters the stress distribution within the concrete, affecting the formation and integrity of the diagonal compression struts. These phenomena, particularly the reinforcement behavior and its impact on stress distribution, are explored in greater detail in the force-displacement curves discussed in the subsequent sections.

Fig. 8 illustrates the minimum principal stress contours for BM3 across the different concrete material models analyzed in this study. The results reveal that the formation of compression struts is notably pronounced in the interior shear spans of the beam compared to the exterior spans. This indicates that the force distribution is more concentrated in the interior spans of these double-span beams, making them more critical in terms of load transfer. Consequently, the reinforcement in the interior shear spans is expected to experience more significant yielding than that in the exterior spans. This observation aligns with the force-flow mechanisms typical of such structural systems and is further explored in detail in the following sections of the study, where the impact of reinforcement and material behavior on the overall structural performance is thoroughly analyzed.

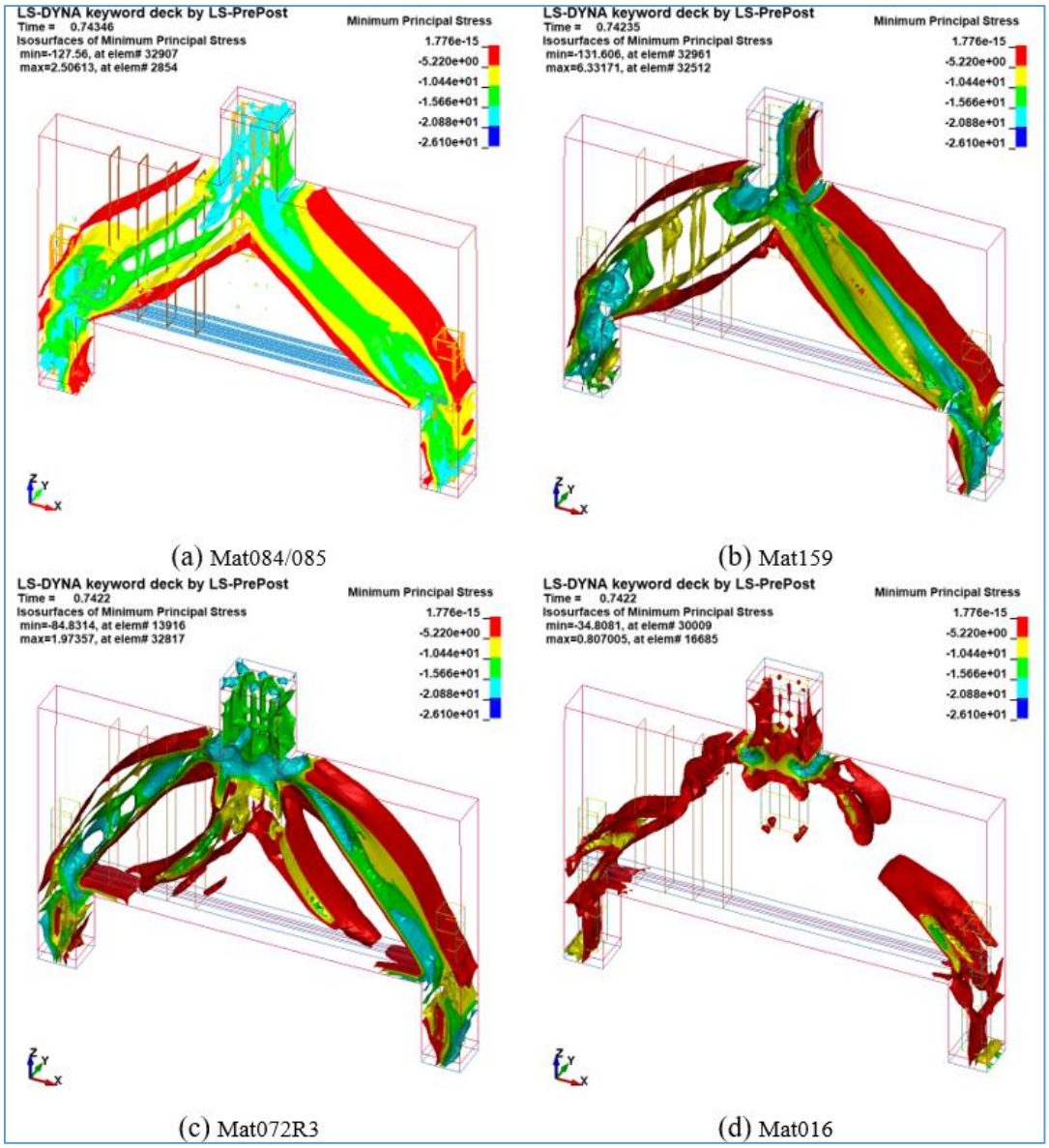

Fig. 7. Minimum principal stress distributions of BM1 at deflection of 7.5mm: (a) Mat084/085; (b) Mat159; (c) Mat072R3; (d) Mat016.

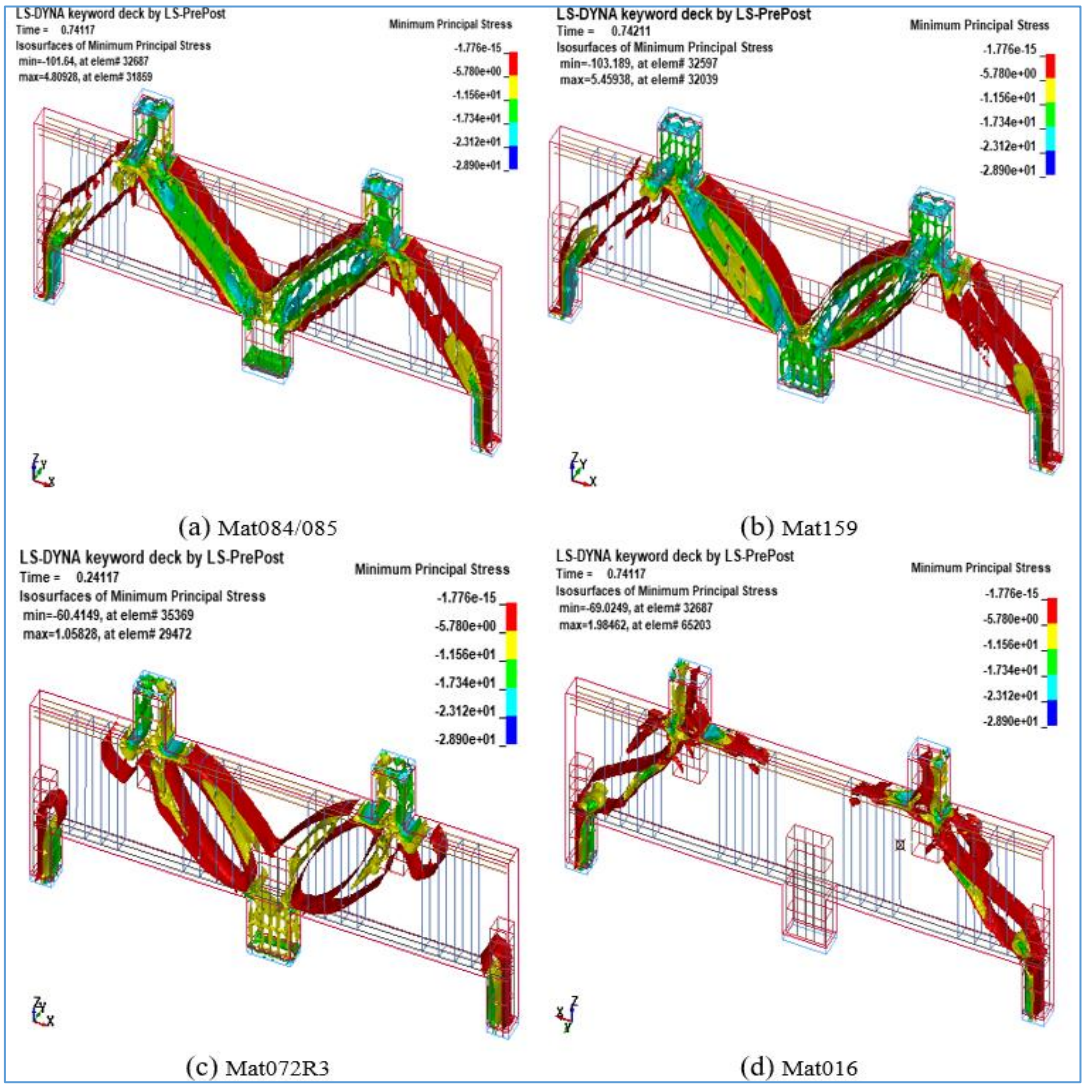

Fig. 8. Minimum principal stress distributions of BM3 at deflections of 7.5mm: (a) Mat084/085; (b) Mat159; (c) Mat072R3; (d) Mat016.

6.1. Global load-displacement response

Fig. 9 shows the shear-deflection response of the numerical simulations for six reference beams (BM1, BM2, BM3, BM4, BM5, and BM6) derived from nonlinear inelastic FE analysis. The behavior of each beam model was assessed using four different concrete material models (specifically, Mat84/85, Mat159, Mat071R3, and Mat16) alongside a single steel material model (Mat003 Plastic Kinematic). Fig. 9 also includes experimentally measured maximum shear strengths of the beams for comparison with the numerical outcomes.

For BM1, the experimentally measured maximum strength was 1204 kN, achieved at a deflection of approximately 5.5 mm. The numerical predictions for maximum shear strength using different material models yielded the following results: Mat084/085 approximated 1190 kN at 5.5 mm deflection, Mat159 predicted 1282 kN at 5 mm, Mat072R3 estimated 1079 kN at 4.7 mm, and Mat016 calculated 1085 kN at 2.5 mm. The discrepancies between these numerically obtained values and the experimental measurement were 1.2%, 6.4%, 10.0%, and 9.8%, respectively.

For BM2, the experimentally measured maximum beam strength was 1500 kN, achieved at a deflection of approximately 6.2 mm. It is important to note that BM2, in contrast to BM1, featured distributed body reinforcement. Regarding the numerical models, using Mat084/085, Mat159, Mat072R3, and Mat016, the predicted maximum shear strengths were approximately 1202 kN at 2.27 mm deflection, 1361 kN at 6.3 mm, 1119 kN at 4.4 mm, and 1110 kN at 5.7 mm, respectively. The discrepancies between these numerically obtained results and the experimentally measured value were about 19.86%, 9.26%, 25.3%, and 25.9%. When comparing the actual strengths of BM1 and BM2, it is observed that the inclusion of body reinforcement in BM2 increased the beam strength from 1204 kN to 1500 kN, indicating a substantial increase of 24.58%. However, this enhancement in strength was not reflected in the numerical results.

For BM3, the experimentally determined maximum strength of the beam was 2170 kN, achieved at a deflection of approximately 6.1 mm. It's noteworthy that BM3 is a continuous beam with shear reinforcement across all four spans. In the numerical models using Mat084/085, Mat159, Mat072R3, and Mat016, the predicted maxi-

mum shear strengths were approximately 1950 kN at 2.27 mm deflection, 2263 kN at 6.3 mm, 1830 kN at 4.4 mm, and 1740 kN at 5.7 mm, respectively. The differences between these numerically obtained results and the experimentally measured value were about 10.13%, 3.83%, 15.66%, and 19.81%, respectively.

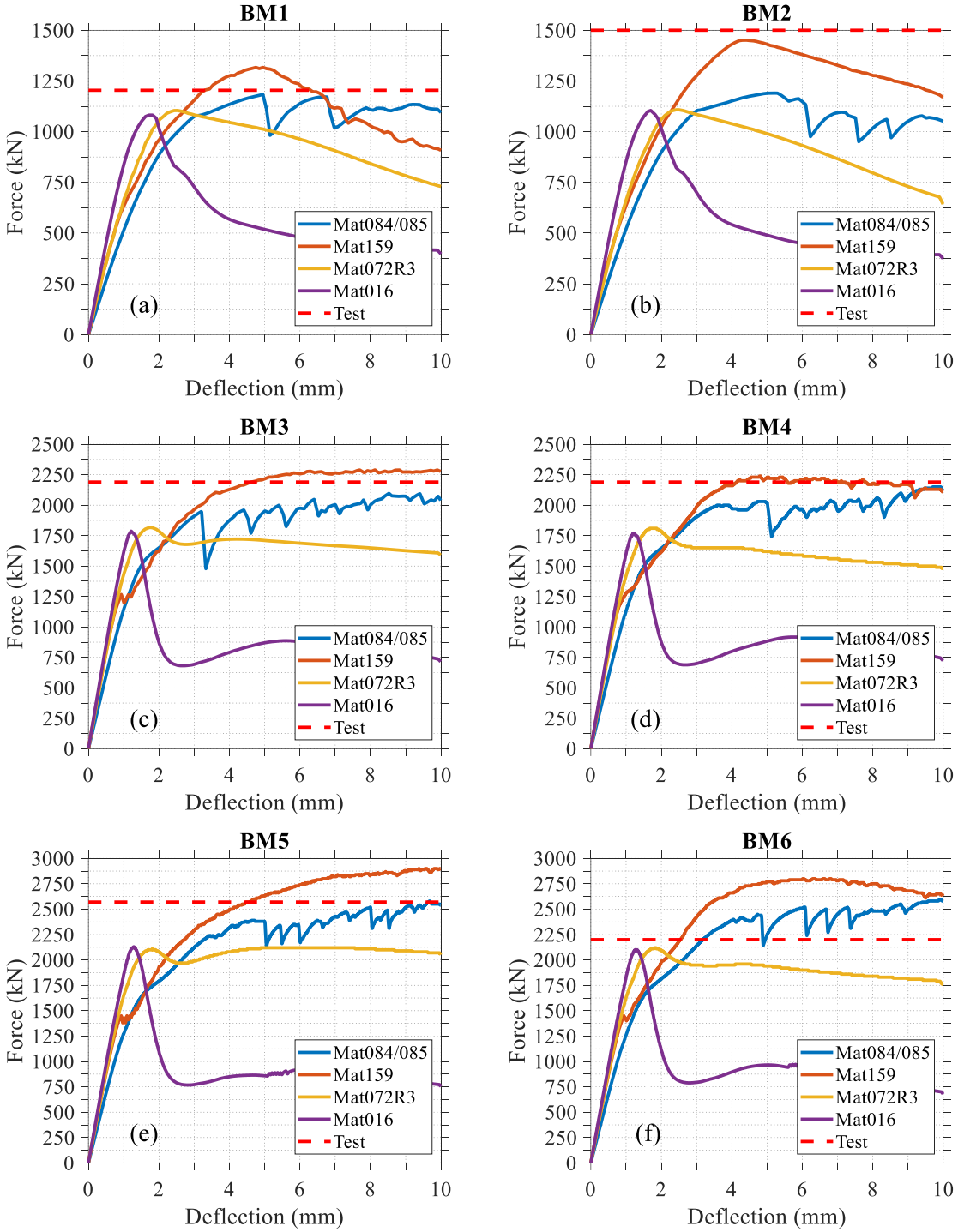

Fig. 9. Shear-deflection curves: (a) BM1;(b) BM2; (c) BM3; (d) BM4; (e) BM5; (f) BM6.

For BM4, the experimentally measured maximum strength of the beam was 2176 kN, achieved at a beam deflection of approximately 7.0 mm. Notably, BM4 is a continuous beam with body reinforcement extending through all spans, but it lacks shear reinforcement. In the numerical models using Mat084/085, Mat159, Mat072R3, and Mat016, the predicted maximum shear strengths were approximately 2035 kN at 5.0 mm deflection, 2240 kN at 6.2 mm, 1810 kN at 2.2 mm, and 1770 kN at 1.7 mm, respectively. The discrepancies between these numerically obtained results and the experimentally measured value were about 6.5%, 2.9%, 16.8%, and 18.7%. Upon comparing the actual strengths of BM3 and BM4, and considering that BM3 used stirrup reinforcement while BM4 used web reinforcement without stirrups, it was observed that stirrups contribute to a greater increase in beam strength than body reinforcement.

For BM5, the experimentally measured maximum strength of the beam was 2571 kN, achieved at a beam deflection of approximately 8.5 mm. It's important to note that, similar to BM4, BM5 is a continuous beam with body reinforcement throughout all spans but lacks shear reinforcement. In the numerical models using Mat084/085, Mat159, Mat072R3, and Mat016, the predicted maximum shear strengths were approximately 2385 kN at 5.0 mm deflection, 2840 kN at 6.1 mm, 2120 kN at 2.1 mm, and 2100 kN at 1.7 mm, respectively. The differences between these numerically obtained results and the experimentally measured value were about 7.2%, 10.5%, 17.5%, and 18.3%. When compared to beams with lighter shear reinforcements, it was observed that the use of heavy stirrups in BM5 significantly enhanced the beam strength.

For BM6, the experimentally measured maximum strength of the beam was 2198 kN, reached at a deflection of approximately 5.5 mm. Notably, BM6 is a continuous beam with heavy horizontal body reinforcement spanning all spans but lacks shear reinforcement. It's also important to acknowledge that the specimen suffered some damage during handling, which might impact the realism of the comparison. Nonetheless, similar numerical model comparisons were conducted for this beam as well. Using the numerical models with Mat084/085, Mat159, Mat072R3, and Mat016, the predicted maximum shear strengths were approximately 2430 kN at 6.0 mm deflection, 2780 kN at 6.1 mm, 2120 kN at 1.8 mm, and 2100 kN at 1.2 mm, respectively. The discrepancies between these numerically obtained results and the experimentally measured value were about 10.6%, 26.5%, 3.5%, and 4.5%.

The observed differences in the results between the material models are due to the inherent mathematical formulations and assumptions underlying each model. These models differ in how they represent concrete behavior under varying loading conditions, including stress-strain relationships, failure criteria, and damage mechanisms.

MAT072R3 (K&C Model) utilizes three failure surfaces to capture yield, maximum, and residual strength. However, it often overestimates the degradation of compressive strength and does not account for stiffness reduction under loading, leading to discrepancies in strength and deformation predictions. MAT084/085 (Winfrith Model), based on a smeared crack approach, assumes elastic-perfectly plastic behavior in compression with bilinear strain softening in tension. While effective in some applications, it may not capture strength degradation under highly nonlinear scenarios. MAT159 (CSCM Model) uses a continuous surface cap model that combines shear failure and hardening compaction surfaces, allowing simulation across a wide range of stress states. Although versatile, it can overestimate parameters like tensile fracture energy. MAT016 (Pseudo-Tensor Model) is a simpler model with lower computational requirements but limited accuracy in capturing complex stress states and nonlinear behavior.

The differences arise primarily due to how each model addresses key aspects of concrete behavior. Advanced models like MAT159 incorporate explicit damage mechanics, whereas others, like MAT084, use smeared approaches. Stress-strain relationships differ in how they handle tension softening, compression hardening, and strain rate effects. Additionally, variations in yield surfaces and failure envelopes significantly influence strength and deformation predictions.

6.2. Axial force demands of stirrups

In this section, axial force demands in the beam stirrups under a range of beam deformations (i.e., Δ=1, 2.5, 3.0, 3.5, 6.0, 10 mm) are examined considering different concrete models. Due to page limitations, the results are discussed using only two beam models: BM1, representing a single-span beam, and BM3, representing a continuous beam. For BM1, the analysis covers the four shear reinforcements located in the left shear span, positioned at distances of 350 mm, 500 mm, 650 mm, and 800 mm from the beam's left end. In the case of BM3, the results pertain to eight shear reinforcements. These are located in both an interior and an exterior shear span of the beam's half symmetric span. Specifically, the shear reinforcements in the exterior shear span are placed at distances of 350 mm, 500 mm, 650 mm, and 800 mm from the left end of the beam. Those in the interior shear span are situated at 1400 mm, 1550 mm, 1750 mm, and 1850 mm from the left end.

For BM1, the axial force distribution for each stirrup is detailed in Fig. 10 to 12, corresponding to the material models Mat084/085, Mat159, and Mat072R3. Notably, results pertaining to Mat016 are excluded, as they were deemed unreasonable. When analyzing the distribution of axial forces in the four shear reinforcements located in the left span of the BM1 model, a notable observation is that the axial forces concentrate in a specific region along the length of the reinforcement. This concentration of axial forces correlates with the diagonal compression strut shape illustrated in Fig. 7. Essentially, the length of the shear reinforcement experiencing the most significant axial force concentration corresponds to the region where the minimum principal stresses occur in the concrete. This indicates a direct relationship between the stress patterns in the concrete and the distribution of axial forces within the shear reinforcements.

When analyzing the axial force demands on the shear reinforcement for different concrete models, it was found that yielding in the reinforcements was most pronounced in the Mat072R3 model, followed by the Mat084/85 model, and least in the Mat59 material. For the Mat159 model, yielding was observed only in the second shear reinforcement (located at X=500mm) at the maximum deformation of 10mm. The other shear reinforcements in this model generally remained within the elastic range. In contrast, for both the Mat84/85 and Mat72 models, the onset of yielding in the shear reinforcement began at approximately 6 mm deformation. In these two material models, yielding was observed in almost all of the four shear reinforcements within the shear span, indicating a more widespread distribution of yielding across the reinforcements in response to beam deformation.

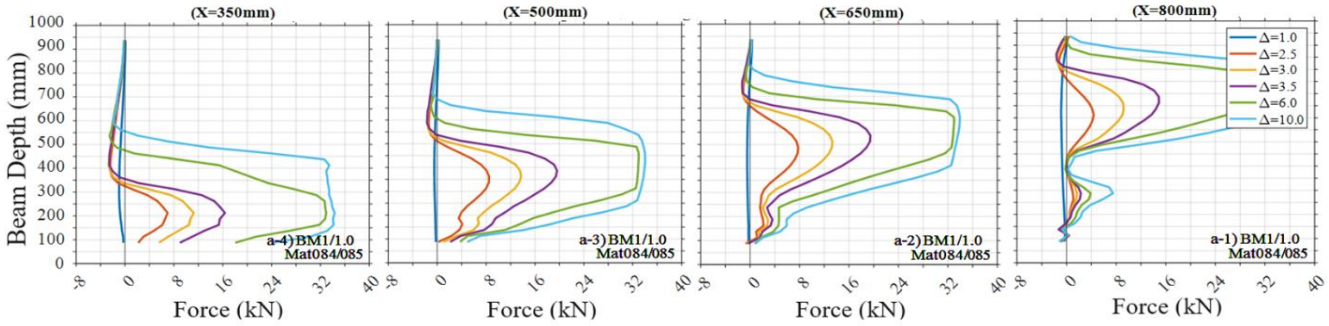

Fig. 10. Axial force demands of stirrups of BM1 using Mat084/085.

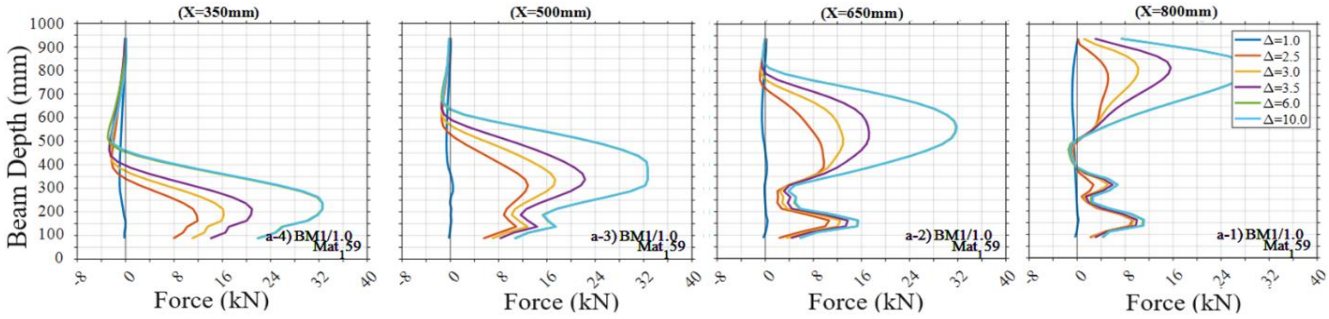

Fig. 11. Axial force demands of stirrups of BM1 using Mat159.

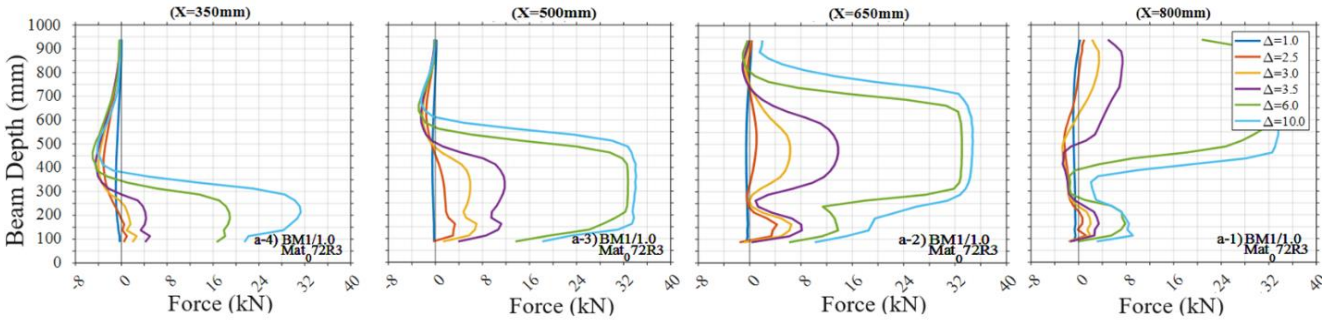

Fig. 12. Axial force demands of stirrups of BM1 using Mat072R3.

For BM1, the axial force distribution for each stirrup is detailed in Fig. 13 to 15 corresponding to the material models Mat084/085, Mat159, and Mat072R3. In the examination of the axial force distribution on the eight shear reinforcements in the first span of the continuous beam BM3 model, a pattern similar to that observed in the BM1 model is evident. The axial forces on the shear reinforcements in BM3 are found to concentrate in specific regions along the lengths of the reinforcements. These areas of concentration align with the pattern of the diagonal compression struts, as depicted in Fig. 8. This observation indicates that, just as in the BM1 model, the regions on the shear reinforcements where axial forces are most intense correspond to the areas where the diagonal compression struts are formed in the concrete.

In the analysis of the axial force demands on the shear reinforcements in the continuous beam BM3 model, a notable distinction is observed between the exterior and interior shear spans. The first four shear reinforcements, located in the exterior span, experience significantly lower axial force demands compared to the subsequent four reinforcements in the interior span. Specifically, for the Mat72 model, the axial force demands on the reinforcements in the exterior span are almost negligible. Regarding the yield ratios in the shear reinforcements: In the exterior span, the highest yielding is seen in the Mat084/85 model, followed by the Mat159 model, and the least in the Mat072R3 model. In the interior span, the highest yielding is observed in the Mat072R3 model, then the Mat84/85 model, and finally, the Mat159 model.

For the shear reinforcements in the interior span across all material models, the yield ratios are predominantly higher in the middle regions of the shear span. Moreover, all reinforcements yield at the maximum beam deformation. In the Mat84/85 and Mat72R3 models, the first yielding in the reinforcements occurs at a beam deformation of 3.5 mm, while in the Mat159 model, it starts at a deformation of 6 mm. In terms of the extent of yielding: In the Mat84/85 and Mat72R3 models, yielding occurs along more than 50% of the reinforcement length. For the Mat159 model, this yielding ratio is around 20%. This analysis highlights the differences in the axial force demands of shear reinforcements in different spans and under various material models, especially in terms of yielding patterns and axial force demands.

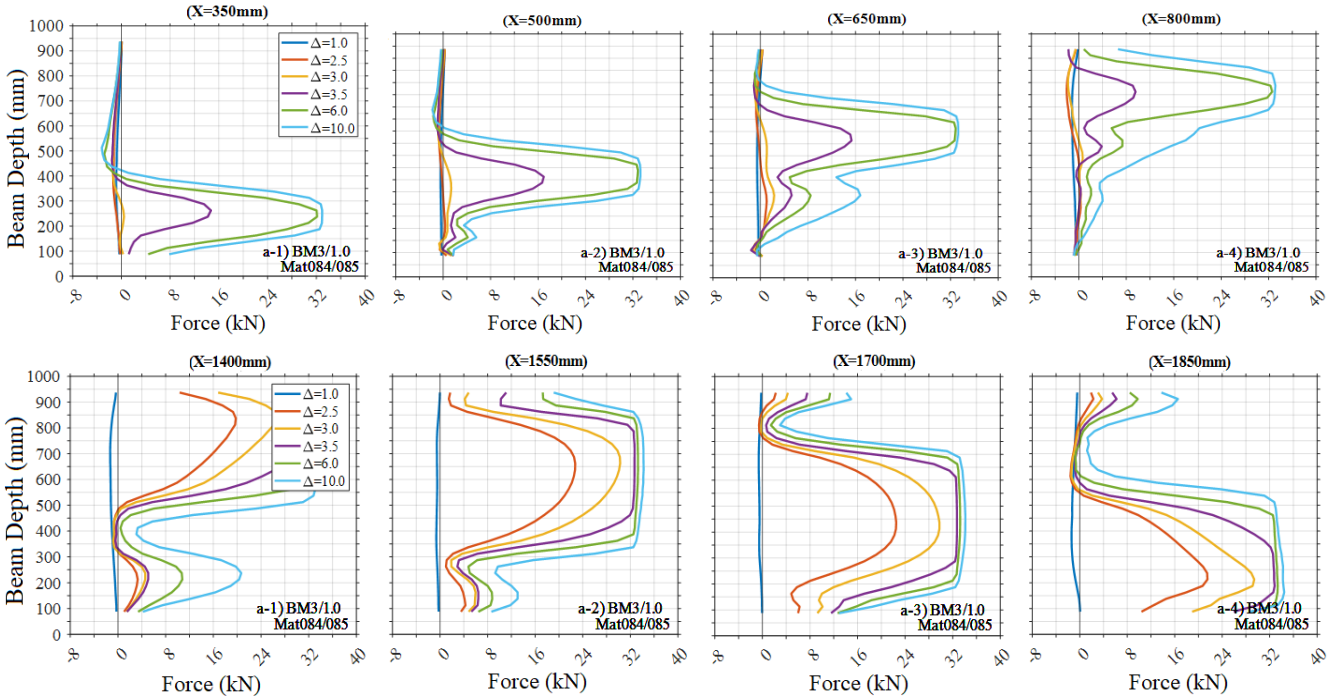

Fig. 13. Axial force demands of stirrups of BM3 using Mat084/085.

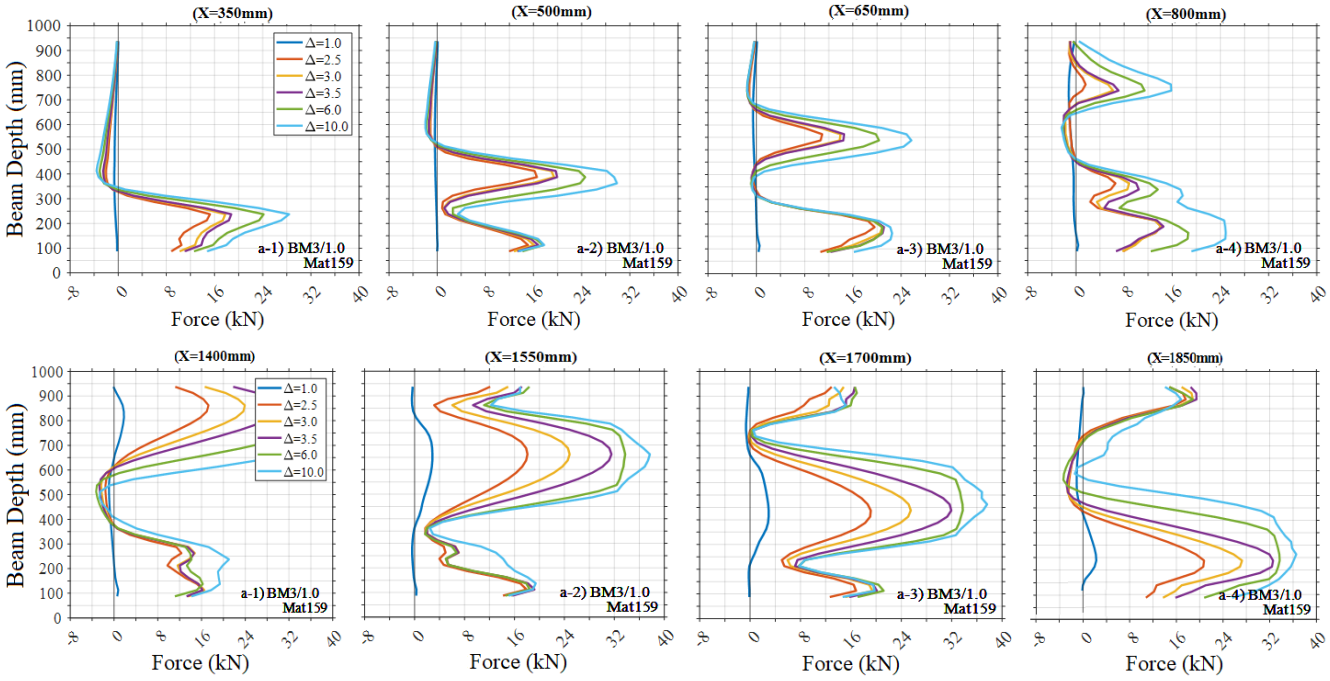

Fig. 14. Axial force demands of stirrups of BM3 using Mat159.

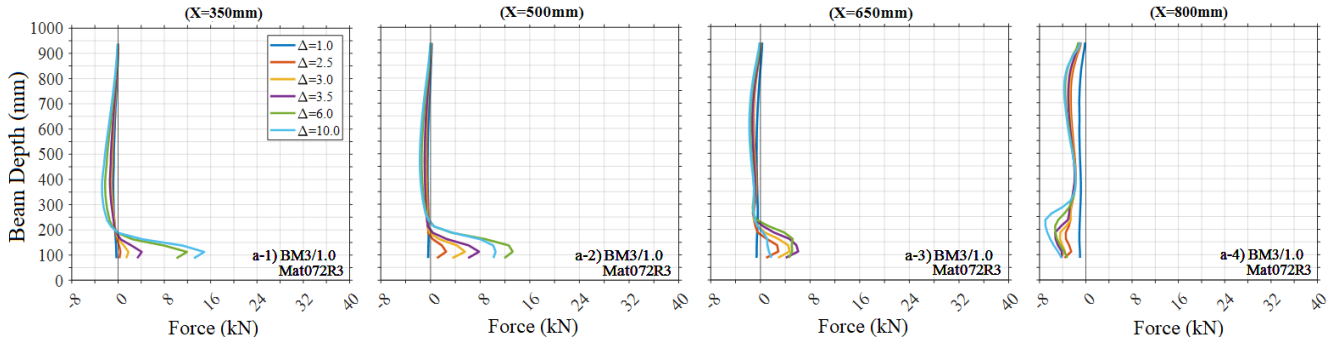

Fig. 15. (continued)

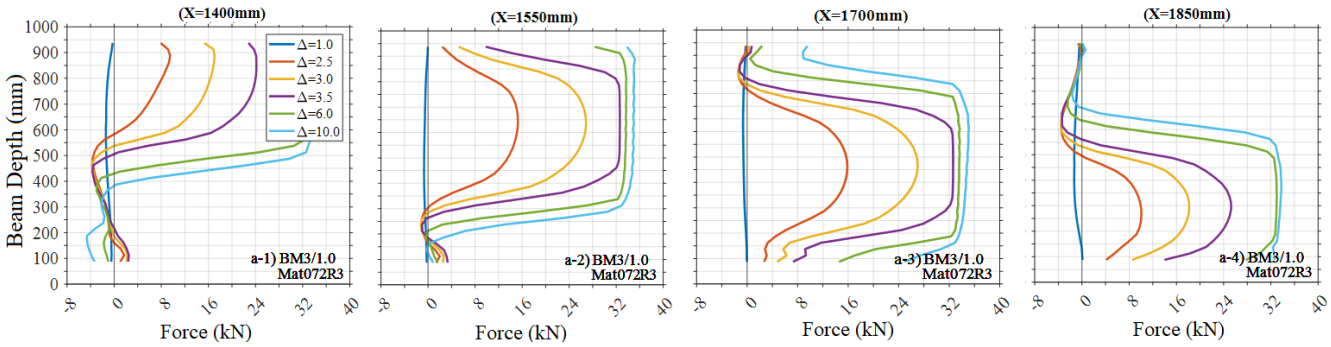

Fig. 15. Axial force demands of stirrups of BM3 using Mat072R3.

The reported findings for the tested beams reveal different patterns of yielding and failure mechanisms: For BM1: Yielding was observed in both the shear and the bottom longitudinal reinforcements before the collapse of the beam. The distribution of tensile force in the longitudinal reinforcement at failure was almost constant, suggesting a uniform stress state along its length. This indicates that both shear and flexural capacities were critical in the failure process; For BM2: Both the shear and longitudinal reinforcements yielded before the beam collapsed. This suggests a combined influence of shear and flexural stresses leading to the failure, similar to BM1; For BM3: Yielding occurred in the main (longitudinal) reinforcement, indicating a flexural failure mechanism. The beam was described as moderately ductile, which implies it underwent significant deformation, typically associated with flexural yielding, before collapsing; For BM4: Yielding in the lower steel reinforcement was noted significantly before the collapse, pointing towards a flexural failure mechanism. This early yielding suggests that the beam's failure was primarily governed by flexural stresses; For BM5: All shear reinforcements yielded, leading to the separation of the struts, indicative of a shear failure. Additionally, the longitudinal reinforcements were under tensile stresses along the entire length of the internal shear spans. However, there was a more pronounced decrease in stress towards the ends of the span compared to the BM3 model, suggesting different stress distributions and possibly different failure mechanisms between the two beams.

6.3. Axial force demands of main reinforcements

In this section, the axial force demands of the longitudinal reinforcement bars located in the bottom regions of the beams were examined for varying beam deformations. The analysis and comparisons are based on the BM1 model, representing a single-span beam, and the BM3 model, representing a continuous beam. To recall the key aspects of the reinforcements in these models: For BM1 (and BM2) there are two rows of bottom reinforcements. Each row consists of 3ϕ20 bars. For BM3 (and BM4, BM5, and BM6) there is only single row of bottom reinforcements, with each row also containing 3ϕ20 bars. The positioning of the reinforcements is such that the center of the first-row reinforcements is located 25 mm above the concrete's outer surface, while the second-row reinforcements are positioned 50 mm above the surface. For BM1, the results are presented as the sum axial force acting on the three bars in a single row. It's noted that the axial force demands on the second-row reinforcements are nearly the same. The average axial force demands of the three bars in a single row are given at beam deflections of Δ=1.0, 2.0, 3.0, 3.5, 6.0, and 10 mm. Note that, the measured tensile strength of the reinforcement materials are 114 kN for models between BM1 to BM4, and 121 kN for models BM5 and BM6. This analysis aims to understand how the axial forces in the longitudinal reinforcements vary under different levels of beam deformation and how these forces are influenced by the reinforcement arrangement and material characteristics in various beam models.

For BM1, the axial force demands on the longitudinal reinforcements under increasing beam deformations are presented in Fig. 16, considering four different concrete materials. The key observations for this model are as follows: For Mat084/85 and Mat159 Models yielding of the reinforcements is observed. The reinforcements remained elastic up to a beam deflection of 6 mm, with yielding commencing after this point. In the Mat084/85 model, about 65% of the longitudinal reinforcements yielded, while in the Mat159 model, 50% yielded. Yielding started from the midspan and spread towards the supports. Near the supports, a decrease in axial force demands was noted, suggesting that the reinforcements remained elastic in these areas. For the Mat072R3 model, the reinforcements stayed elastic throughout the entire beam length. However, the axial force demands decreased from the midspan towards the supports. The axial forces reached about 70% of the yield strength of the reinforcements. For the Mat016 model, after a beam deflection of 2 mm, the axial force demands on the longitudinal reinforcements remained constant along the entire length of the beam. These forces corresponded to approximately 30% of the yield strength of the reinforcements. These findings indicate a significant variation in the behavior of the longitudinal reinforcements under different concrete models and beam deformations.

For BM3, the axial force demands on the longitudinal reinforcements under increasing beam deformations are presented in Fig. 17, considering four different concrete materials. The single bar yield strength for this beam is 114 kN, resulting in a total yield force of 342 kN for the bottom row of beam reinforcement. Yielding occurred in all models that used the four different concrete materials.

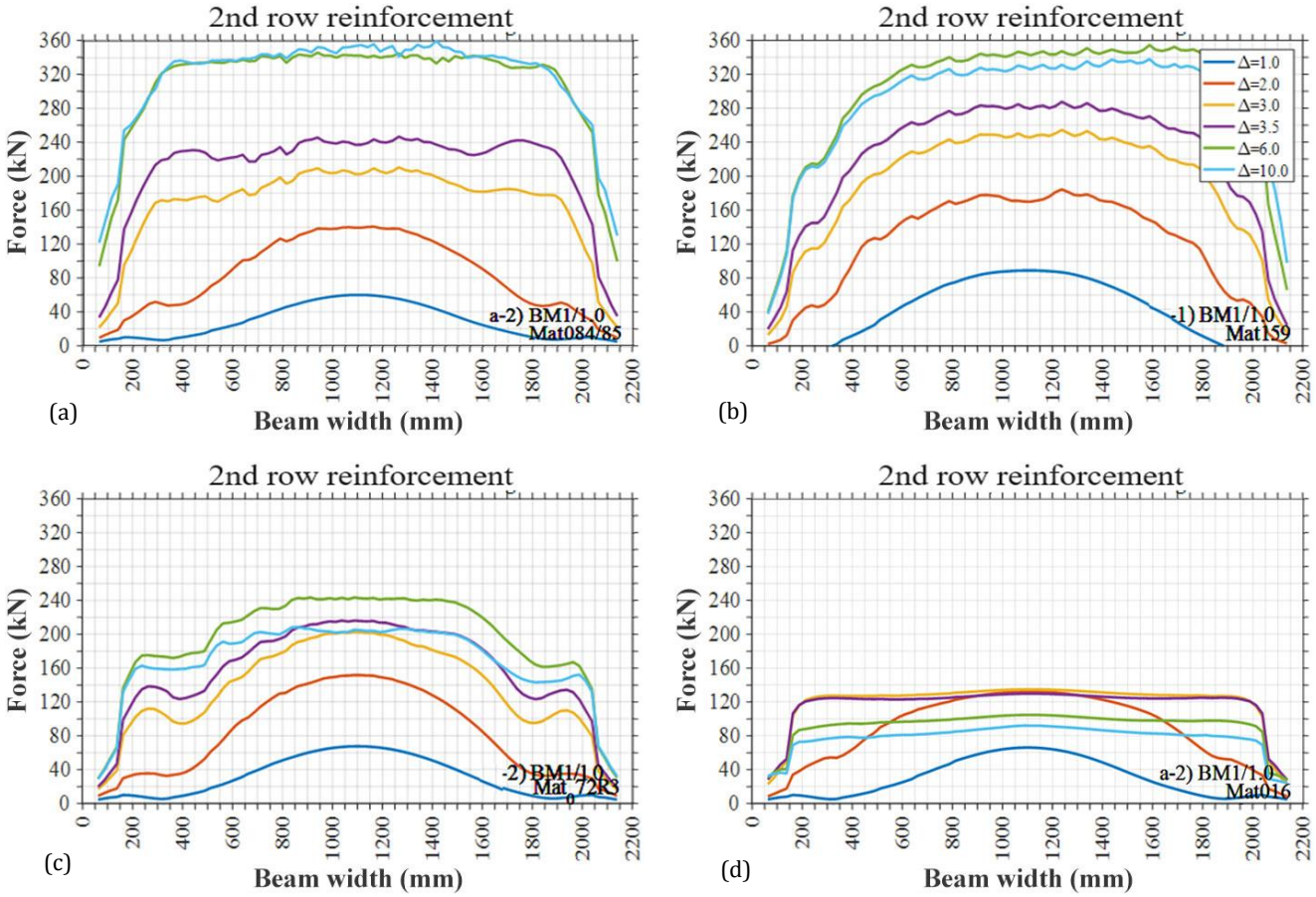

Fig. 16. Axial force demands of longitudinal reinforcement of BM1:
(a) Mat084/085; (b) Mat159; (c) Mat072R3; (d) Mat016.

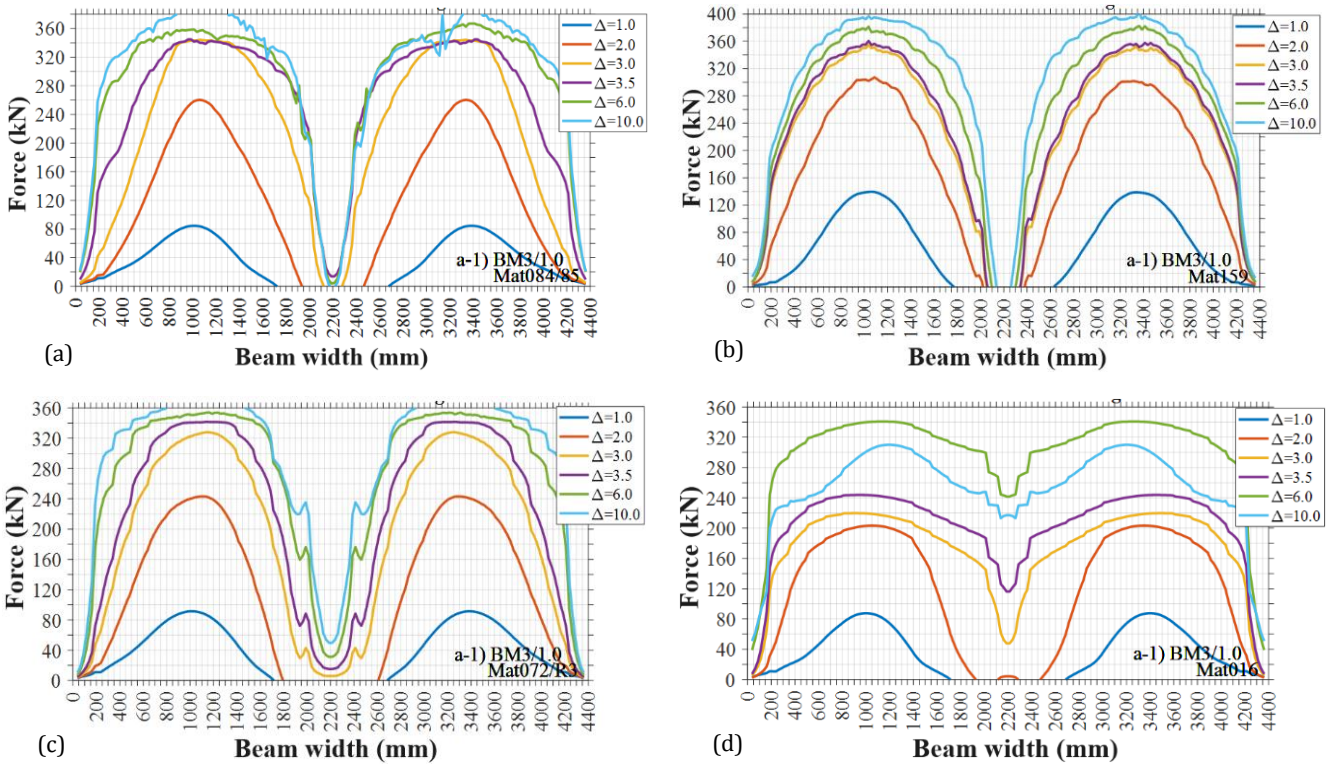

Fig. 17. Axial force demands of longitudinal reinforcement of BM3:
(a) Mat084/085; (b) Mat159; (c) Mat072R3; (d) Mat016.

In the Mat084/85, Mat159, and Mat072R3 models, yielding in the reinforcements started at approximately 3.5 mm beam deformation. The axial force demands in the reinforcements of these three models showed similar behavior along the beam length, with axial force distributions being generally symmetric across both spans. In these models, the axial force demand in the reinforcements reached its peak in the midspan of the beam spans, then decreased and approached zero towards the mid-span and end supports. In contrast, the Mat016 model displayed a different behavior, with reinforcement yielding observed only under high beam deflection, specifically at 10 mm. The distribution of axial force demands in the reinforcements along the beam length in this model was different from the other three models. While the other three concrete models had almost zero axial force demand in the central support region, the reinforcements in this region in the Mat016 model experienced some level of force demand.

These observations indicate a range of behaviors in the longitudinal reinforcements under varying concrete models and beam deformations. The yielding patterns, axial force demands, and their distribution along the beam length vary significantly, reflecting the influence of concrete material properties and the structural response to loading.

7. Conclusions

This study presents an efficient and cost-effective method for evaluating the shear capacity of reinforced concrete deep beams using LS-DYNA, offering a reliable alternative to extensive experimental testing. The analysis of four different concrete models provided insights into the most accurate approaches for predicting beam capacities. These findings can be important for enhancing the resilience of critical urban infrastructure, such as bridges and foundations. By optimizing deep beam designs, engineers can create more durable, disaster-resistant structures, contributing to the long-term sustainability and safety of rapidly growing cities. The study has the following outcomes:

- Significant differences in strength predictions and the distribution of reinforcement forces among different material models were observed. Among the various materials used, the Mat159 model provided the most accurate estimate of the experimentally measured beam shear strength. While the beam strengths obtained with this material are on the conservative side, the percentage differences between the computational results and the values measured in experimental studies were found to be 6.4%, 9.3%, 3.8%, 2.9%, and 10.5% for BM1, BM2, BM3, BM4, BM5, respectively. For BM6, the difference was notably higher at 26.5%. It is important to note that the BM6 model experienced damage during the test setup. Moderate prediction was achieved using the Mat084/85 model. The analysis results obtained using the Mat072R3 and Mat016 models underestimated the measured beam carrying capacity values. The analysis results obtained using the Mat016 model exhibited very poor performance in predicting the measured beam carrying capacity, as well as the principal stress distributions within the beam and the axial force demands on the beam reinforcements.
- Similar to the findings in experimental studies, an analysis of the minimum principal stress distributions in the beams showed that a truss mechanism, made up of struts, was formed regardless of the amount and configuration of reinforcement. However, it was observed that the struts in double-span beams were more prominently developed in the interior spans as compared to the exterior spans. This finding suggests that in two-span deep beams, the inner spans are more critical than the outer spans and should be reinforced with more shear reinforcement.
- The minimum principal stresses in the diagonal compression struts along the shear span did not exceed the concrete's compressive strength, yet stress concentrations are found near the strut ends at the top and bottom surfaces of the beam, aligns with experimental findings. This highlights the importance of these areas, as crushing in concrete is typically observed in these regions of the struts.
- The numerical analyses results showed that the longitudinal reinforcement in the beams does not contribute to the beam strength, while an increase in the amount of shear reinforcement does enhance beam strength. This outcome of the numerical models is consistent with experimental findings.
- When examining the axial force demands on the shear reinforcement for different concrete models, yielding in the reinforcements is observed most prominently in the Mat072R3 model, followed by the Mat084/85 model, and finally, the Mat159 material. It has been observed that the yielding of shear reinforcements occurred within the dimensions of the diagonal compression struts observed in the principal stresses of concrete. Outside these dimensions, the shear reinforcements remained elastic. This finding is important as it indicates the localized nature of yielding in shear reinforcements and highlights the significance of the diagonal compression struts in the structural behavior of reinforced concrete beams.
- When analyzing the axial force demands on the bottom longitudinal reinforcements of beams for different concrete models, it was found that these demands are consistent with experimental observations. Upon examining the axial force demands on the bottom longitudinal reinforcements of single-span beams for various concrete models, it was noted that the reinforcement yielded in the models using Mat159 and Mat072R3. In contrast, the reinforcement remained elastic in the models utilizing Mat084/085 and Mat016. In the case of double-span beams, however, reinforcement yielding was observed in all the material models used.
- The study's primary objective—predicting the strength values of reinforced concrete deep beams—was comprehensively addressed through detailed analyses and validations. The comparison of numerical results with experimental data demonstrates the effectiveness of the proposed methodology in accu-

rately estimating shear strength values. Mat159 emerged as the most reliable concrete model for strength prediction, achieving close alignment with experimental measurements across all beam types. This accuracy highlights the method's potential as a robust tool for predicting beam capacities.

- The methodology employed in this study can be readily adapted for beams with different geometries, materials, or loading conditions by recalibrating material models and boundary conditions. This flexibility enhances the applicability of the findings, saving time for researchers and practitioners alike. Furthermore, disseminating these results to the broader research community enables critical evaluation and comparison, fostering the refinement of existing methods.

By employing LS-DYNA's default concrete parameter options, this study established a cost-effective, reliable method for deep beam capacity estimation, reducing the need for extensive experimental testing. This approach facilitates the exploration of deep beams with various configurations without significant experimental investments.

Acknowledgements

The research presented in this article is an expansion of the work originally conducted in the M.Sc. thesis of Gökhan Karaman.

Funding

The authors received no financial support for the research, authorship, and/or publication of this manuscript.

Conflict of Interest

The authors declared no potential conflicts of interest with respect to the research, authorship, and/or publication of this manuscript.

Author Contributions

All of the authors made substantial contributions to conception and design, or acquisition of data, or analysis and interpretation of data; were involved in drafting the manuscript or revising it critically for important intellectual content; and gave final approval of the version to be published.

Data Availability

The datasets created and/or analyzed during the current study are not publicly available, but are available from the corresponding author upon reasonable request.

REFERENCES

ACI 318-19 (2019). Building code requirements for structural concrete. American Concrete Institute, Farmington Hills, MI.

ACI 318-83 (1983). Building code requirements for reinforced concrete. American Concrete Institute, Detroit, MI.

Arabzadeh A (2020). Analysis of boundary condition effects on RC deep beams. *Structures*, 23, 821-830.

ASCE-ACI Committee 445 on Shear and Torsion (1998). Recent approaches to shear design of structural concrete. *Journal of Structural Engineering*, 124(12), 1375-1417.

Broadhouse B (1995). The Winfrith concrete model in LS-DYNA3D. *Report: SPD/D (95)*, 363.

Broadhouse B, Neilson A (1987). Modelling reinforced concrete structures in DYNA3D. Safety and Engineering Science Division, UKAEA Atomic Energy Establishment, Winfrith, UK.

CSA A23.3 (2004). Design of concrete structures. Canadian Standard Association, Mississauga, ON.

Chen H, Yi W-J, Ma ZJ (2020). Shear-transfer mechanisms and strength modeling of RC continuous deep beams. *Journal of Structural Engineering*, 146(11), 04020240.

Chen H, Yi W-J, Ma ZJ, Hwang H-J (2019). Shear Strength of Reinforced Concrete Simple and Continuous Deep Beams. *ACI Structural Journal*, 116(6), 31-40.

Collins MP, Bentz EC, Sherwood EG (2008). Where is shear reinforcement required? Review of research results and design procedures. *Structural Journal*, 105(5), 590-600.

Gedik YH, Nakamura H, Yamamoto Y, Ueda N, Kunieda M (2012). Effect of stirrups on the shear failure mechanism of deep beams. *Journal of Advanced Concrete Technology*, 10(1), 14-30.

Grassl P, Johansson M, Leppänen J (2018). On the numerical modelling of bond for the failure analysis of reinforced concrete. *Engineering Fracture Mechanics*, 189, 13-26.

Imani R, Mosqueda G, Bruneau M (2015). Experimental study on post-earthquake fire resistance of ductile concrete-filled double-skin tube columns. *Journal of Structural Engineering*, 141(8), 04014192.

Jiang H, Zhao J (2015). Calibration of the continuous surface cap model for concrete. *Finite Elements in Analysis and Design*, 97, 1-19.

Li Z, Liu X, Kou D, Hu Y, Zhang Q, Yuan Q (2023). Probabilistic models for the shear strength of RC deep beams. *Applied Sciences*, 13(8), 4853.

LS-DYNA version R10.0 (2017). Livermore Software Technology Corporation, Livermore, CA.

LSTC (2017). LS-DYNA Keyword User's Manual, Volume II, Material Models. Livermore Software Technology Corporation, Livermore, CA.

Ma C, Wang S, Zhao J, Xiao X, Xie C, Feng X (2023). Prediction of shear strength of RC deep beams based on interpretable machine learning. *Construction and Building Materials*, 387, 131640.

Markovich N, Kochavi E, Ben-Dor G (2011). An improved calibration of the concrete damage model. *Finite Elements in Analysis and Design*, 47(11), 1280-1290.

Marti P (1985). Basic tools of reinforced concrete beam design. *Journal Proceedings*, 82(1), 46-56.

Murray YD, Abu-Odeh AY, Bligh RP (2007). Evaluation of LS-DYNA concrete material model 159. Office of Research, Development, and Technology, Federal Highway Administration, United States.

Novozhilov YV, Dmitriev AN, Mikhaluk DS (2022). Precise calibration of the continuous surface cap model for concrete simulation. *Buildings*, 12(5), 636.

Polat E (2020a). Investigation of concrete filled composite plate shear walls using finite element methods. *Uludağ University Journal of the Faculty of Engineering*, 25(1), 139-152.

Polat E (2020b). Investigation of influence of concrete material models on cyclic inelastic response of a concrete filled composite plate shear wall. *Challenge Journal of Structural Mechanics*, 6(2), 91-98.

Polat E (2022a). Theoretical Models for Tie Bar Maximum Axial Force Demand in Composite Plate Shear Walls–Concrete Filled. *International Journal of Steel Structures*, 22(4), 1108-1125.

Polat E (2022b). Boundary plate influence on tie bars axial force demands in composite plate shear walls–concrete filled. *Challenge Journal of Structural Mechanics*, 8(4), 166-172.

Polat E, Bruneau M (2017). Modeling cyclic inelastic in-plane flexural behavior of concrete filled sandwich steel panel walls. *Engineering Structures*, 148, 63-80.

Polat E, Bruneau M (2018). Cyclic inelastic in-plane flexural behavior of concrete filled sandwich steel panel walls with different cross-section properties. *Engineering Journal, American Institute of Steel Construction*, 55, 45-76.

Polat E, Kenarangi H, Bruneau M (2021). Investigation of tie bars axial force demands in composite plate shear walls—concrete filled. *International Journal of Steel Structures*, 21, 901-921.

Polat E, Polat EG (2024). Predicting and optimizing maximum flexural strength of planar composite plate shear walls – concrete filled with the application of LR and RSM. *Structures*, 69, 107353.

Rogowsky D, McGregor J, Ong S (1986). Tests of reinforced concrete deep beams. *Journal of the American Concrete Institute*, 83(4), 614-623.

Schlaich J, Schäfer K, Jennewein M (1987). Toward a consistent design of structural concrete. *PCI Journal*, 32(3), 74-150.

Tang R-Y, Sun Y-L, Wang Y-G, Ding R, Fan J-S, Nie J-G (2024). Finite element analysis of single steel-plate concrete composite containment of nuclear power plant under commercial aircraft impact. *Engineering Structures*, 321, 118998.

Tay SK, Poon JK, Chan R (2016). Modeling rebar in reinforced concrete for ALE simulations. *14th International LS-DYNA Users Conference,* Detroit, MI, 1-14.

Winkelbauer BJ (2015). Phase I Evaluation of Selected Concrete Material Models in LS-DYNA. *M.Sc. thesis*, University of Nebraska-Lincoln, Lincoln, NE.

Wittmann F, Rokugo K, Brühwiler E, Mihashi H, Simonin P (1988). Fracture energy and strain softening of concrete as determined by means of compact tension specimens. *Materials and Structures*, 21(1), 21-32.

Wu Y, Crawford JE, Magallanes JM (2012). Performance of LS-DYNA concrete constitutive models. *12th International LS-DYNA Users Conference,* Dearborn, MI, 3-5.

Wu Y, Crawford JE (2015). Numerical modeling of concrete using a partially associative plasticity model. *Journal of Engineering Mechanics*, 141(12), 04015051.

Youssf O, ElGawady MA, Mills JE (2015). Displacement and plastic hinge length of FRP-confined circular reinforced concrete columns. *Engineering Structures*, 101, 465-476.

Zargarian M, Rahai A (2022). An experimental and numerical study on continuous RC deep beams strengthened with CFRP strips. *International Journal of Civil Engineering*, 20(6), 619-637.

Zhao M-Z, Lehman DE, Roeder CW (2021). Modeling recommendations for RC and CFST sections in LS-DYNA including bond slip. *Engineering Structures*, 229, 111612.